Research Square

Preprints are preliminary reports that have not undergone peer review.
They should not be considered conclusive, used to inform clinical practice,
or referenced by the media as validated information.

Long-term seismic background level variations reveal volcanic fluid supply and serve as a sensitive indicator for volcano monitoring at Kusatsu-Shirane volcano, Japan

Tsukasa KOBAYASHI

kobayashi-tsukasa@onken.odawara.kanagawa.jp

Kanagawa-ken https://orcid.org/0009-0005-6013-6289

Mie Ichihara

University of Tokyo: Tokyo Daigaku

Akihiko Terada

Tokyo Tech: Tokyo Kogyo Daigaku

Kenji Nogami

Tokyo Kogyo Daigaku

Yohei Yukutake

University of Tokyo: Tokyo Daigaku

Research Article

Keywords: Seismic background level (SBL), Kusatsu-Shirane Volcano, Volcanic unrest, phreatic eruption, hydrothermal system, volcano monitoring

Posted Date: March 10th, 2026

DOI: https://doi.org/10.21203/rs.3.rs-8859259/v1

License: This work is licensed under a Creative Commons Attribution 4.0 International License.
Read Full License

Title page:

Title: Long-term seismic background level variations reveal volcanic fluid supply and serve as a sensitive indicator for volcano monitoring at Kusatsu-Shirane volcano, Japan

Author #1: Tsukasa Kobayashi, Japan Meteorological Agency, Present address: Hot Springs Research Institute of Kanagawa Prefecture, 586 Iriuda, Odawara, Kanagawa, Japan, kobayashi-tsukasa@onken.odawara.kanagawa.jp

Author #2: Mie Ichihara, The Earthquake Research Institute, The University of Tokyo, Tokyo, 113-0032, Japan, ichihara@eri.u-tokyo.ac.jp

Author #3: Akihiko Terada, Volcano and Earthquake Research Division, Multidisciplinary Resilience Research Center, Institute of Integrated Research, Institute of Science Tokyo, 2-12-1 Ookayama, Meguro, Tokyo, 152-8551, Japan, terada@ksvo.titech.ac.jp

Author #4: Kenji Nogami, Volcano and Earthquake Research Division, Multidisciplinary Resilience Research Center, Institute of Integrated Research, Institute of Science Tokyo, 2-12-1 Ookayama, Meguro, Tokyo, 152-8551, Japan,

knogami@ksvo.titech.ac.jp

Author #5: Yohei Yukutake, Earthquake Research Institute, The University of Tokyo, 1-1-1 Yayoi, Bunkyo-ku, Tokyo, Japan, yukutake@eri.u-tokyo.ac.jp

Indicate the corresponding author

Tsukasa Kobayashi

Abstract

Kusatsu-Shirane volcano in central Japan has repeatedly experienced phreatic eruptions, with the Yugama crater being one of the main centers of activity. To clarify long-term variations in volcanic activity around the Yugama crater, we analyzed more than 20 years of continuous seismic records using a statistical approach to calculate the Seismic background level (SBL). This method enables the detection of weak volcanic signals that are buried in background noise. The results revealed that SBL increased during the unrest episodes in 2014 and 2018, with a strong correlation with both deep and shallow sources of ground deformation. These SBL increases are interpreted as reflecting changes in volcanic activity associated with the supply of volcanic fluids from deeper to shallower regions within the volcanic system. The SBL ratio between stations also changed during these unrest periods, indicating differences in the spatial distribution of the SBL vibration source. Variations in SBL were also detected during non-unrest periods, coinciding with minor surface phenomena such as color changes of the Yugama crater lake and the appearance of new fumaroles. These correspondences imply that the SBL reflects even subtle fluctuations in volcanic and hydrothermal activity

without strong seismic or deformation signals. Overall, this study demonstrates that SBL analysis provides a sensitive and quantitative means of detecting weak volcanic signals associated with subsurface fluid activity. Although SBL analysis alone cannot replace conventional monitoring techniques, it offers a powerful tool for detecting subtle variations in volcanic activity. When combined with SBL ratio and particle motion analyses, it also provides spatial information about the vibration source, thereby improving volcano monitoring in hydrothermal and phreatic-eruption environments.

Keywords

Seismic background level (SBL), Kusatsu-Shirane Volcano, Volcanic unrest, phreatic eruption, hydrothermal system, volcano monitoring

Main Text

1.Introduction

Long-term analysis of seismic data is important, because the evaluation of volcanic activity is difficult to achieve using individual datasets alone. Combining various observations provides a more reliable picture of the state of a volcano (Poland and Anderson 2020; Burchardt et al. 2022; Acocella et al. 2024; Stix et al. 2025). Recent studies have shown that an eruption forecasting model using data from multiple sensors or data streams with the Bayesian network method performs better than models using any single dataset (Behr et al. 2025).

In recent years, attempts have been made to detect weak volcanic seismic signals buried in background noise and to track volcanic activity through long-term analysis. Ichihara et al. (2023) statistically processed seismic waveforms recorded during the nighttime period with low noise levels and defined the daily Seismic background level (SBL). They extracted weak volcanic signals (SBL vibrations) , which increased several months before the eruptions of Shinmoe-dake, an active cone of the Kirishima volcanic group in southern Kyushu, Japan. GNSS analysis also detected inflation several months

before the eruptions, but the deformation source was located deep and away from Shinmoe-dake. The SBL signals are inferred to have originated from shallow regions directly beneath the volcano, and the fact that such weak signals were detected several months in advance is particularly significant. Ichihara et al. (2023) suggested that SBL amplitude variations may reflect changes in the state of the subsurface hydrothermal system or aquifer caused by interactions with magmatic fluids, and that SBL can serve as a new indicator for volcano monitoring.

The SBL analysis is also useful for understanding the behavior of shallow fluids even in volcanic environments where phreatic eruptions occur. Kurihara (2023) applied the SBL analysis and detected signals associated with the 2015 phreatic eruption at Hakone volcano. Stix and De Moor (2018) proposed two conceptual models for phreatic eruptions and discussed the heating processes of hydrothermal systems and near-surface aquifers caused by the supply of volcanic fluids prior to eruption. Because a well-developed hydrothermal system exists beneath the Yugama crater at Kusatsu-Shirane volcano (Hirabayashi 1999; Terada 2018), detecting variations in the subsurface hydrothermal system is crucial for understanding the state of volcanic activity.

At Kusatsu-Shirane volcano, recent activity is dominated by phreatic eruptions (Terada 2018; Ishizaki et al. 2025). There, long-term evaluations of volcanic activity have been conducted through various types of observations, such as geochemical monitoring of lake water in the Yugama crater and adjacent Fumarolic gases (Ohba and Yaguchi 2025) and geomagnetic measurements (Takahashi and Fujii 2014; Kanda et al. 2025).

Seismic observations also have a long history. Continuous monitoring has been conducted since the Japan Meteorological Agency (JMA) installed a seismometer in 1978 (Yamasato 2005). Some seismic instruments have been operated very close to the Yugama crater, making the area an excellent field site for studying phreatic eruptions. However, studies using seismometer data have mainly focused on short-term earthquake features. For example, Kumagai et al. (2002a) analyzed long-period (LP) events and discussed temporal changes in the physical properties of fluid in cracks beneath the Yugama crater lake from August 1992 to January 1993. Long-term evaluations of volcanic activity of Kusatsu-Shirane using seismic data remain insufficient.

In this study, we analyzed more than 20 years of seismic data recorded around the Yugama crater. As a result, we identified, for the first time, the presence of SBL

vibrations beneath the Yugama crater. The aim of this study is to clarify how the SBL correspond to volcanic activity. This understanding will improve our knowledge of the relationship between the supply of volcanic fluids and the shallow aquifer or hydrothermal system in a phreatic-eruption environment.

2. Background of Kusatsu-Shirane Volcano

2.1 Geological setting

Kusatsu-Shirane volcano, an active volcano located in the north-western part of Gunma Prefecture, consists of a group of pyroclastic cones including Shirane, Ainomine, and Motoshirane, which are aligned in a north–south direction (Fig. 1a). At the northernmost cone lies the Yugama crater lake, around which phreatic eruptions have frequently occurred (Terada 2018; Ishizaki et al. 2025).

2.2 Recent activity (2014-2023)

Since 2014, Kusatsu-Shirane volcano has experienced episodes of volcanic unrest that might have been driven by a supply of volcanic fluids from deeper levels of the system (Munekane 2021). In both 2014 and 2018, seismic activity markedly increased around

118 the Yugama crater (Fig. 1b), accompanied by inflation directly beneath the crater
119 (Terada et al. 2025). Analyses of regional GNSS measurements revealed an inflation
120 source located a few kilometers northwest of the Yugama crater at a depth of
121 approximately 4 km. The inflation at this deep source began before the onset of both the
122 2014 and 2018 unrests (Munekane 2021).
123 The 2018 unrest was particularly close to a pre-eruptive condition, as indicated by
124 several precursory signals. A rapid increase in seismic activity around Yugama was
125 observed on 22 April 2018, accompanied by a crustal deformation signal. Tiltmeter
126 observations indicated a pressure source located to the west of Yugama (JMA 2018a, b;
127 Terada et al. 2021, 2025). The hypocenters of volcano-tectonic (VT) earthquakes
128 became progressively shallower with time (Kobayashi et al. 2019). During this activity,
129 a very-long-period (VLP) earthquake, which is regarded as an important tool for
130 assessing the probability of a future eruption (Stix and De Moor 2018; Niu and Song
131 2020; Takeo et al. 2022), was recorded, followed by the reversed change of the tilt trend
132 and the gradual decrease of the seismic activity (JMA 2018a, b). The occurrences of a
133 VLP earthquake and migration of VT-earthquake hypocenters suggested that the

134 volcanic system was close to eruption. Another similar episode of sudden intensification
135 of seismic activity occurred in late September 2018.
136 In June 2018, a dark-colored change was observed on the surface of the Yugama crater
137 lake (JMA 2018c; Terada and Kuwahara 2025). A dark-colored change on the surface of
138 a lake had been observed in the past. In January 1989, similar black floating materials
139 were observed on the lake surface, which were interpreted as evidence of a sudden
140 discharge of volcanic gas and hydrothermal fluid beneath the lake surface (Ida et al.
141 1989).
142 Although no eruption occurred around the Yugama crater during each unrest, a phreatic
143 eruption took place at Motoshirane, located about 2 km south of the Yugama, in January
144 2018 (Kametani et al. 2025). Munekane (2021) suggested that a deep deformation
145 source may have influenced the volcanic activities at the Yugama crater and possibly
146 the eruption at Motoshirane through the shallow hydrothermal fluid reservoir (C2a)
147 identified by Matsunaga et al. (2020a, b).
148 These observations indicate that detailed analyses of the 2014 and 2018 episodes of
149 volcanic unrest are crucial for understanding the activity of Kusatsu-Shirane volcano

and the mechanisms of phreatic eruptions.

2.3 Long-term observation (late 1990s-2023)

When focusing on the 30-years trend of seismicity, the number of earthquakes has gradually increased since the early 2000s (Fig. 1b). In addition, several surface phenomena have been observed around the Yugama crater, including the appearance of a water jet, color changes on the surface of the Yugama crater lake, as indicated by blue triangles in Fig. 1b (Volcanic Fluid Research Center, Tokyo Institute of Technology 2004; JMA 2013), and the emergence of new fumaroles around the crater, as indicated by yellow squares in Fig. 1b (JMA 2008a, b, 2013).

These facts suggest that, after a relatively quiet period following the early 1990's activity, volcanic activity gradually intensified and eventually culminated in the 2014 and 2018 unrests. Therefore, analyzing and interpreting volcanic activity in decades, including the period before the 2014 unrest, is essential for interpreting the 2014 and 2018 unrests and for characterizing the baseline behavior of Kusatsu-Shirane volcano as a site of phreatic eruptions.

3. Data and methods

3.1 Data

We analyzed data from short-period seismometers installed near the Yugama crater by the JMA and the Tokyo Institute of Technology (Reorganized to Institute of Science Tokyo in October 2024) (Fig. 2). The installation depths of the seismometers are as follows: KSHA is installed on the ground surface, KSAO at a depth of 95 m, KSE at 50 m, KSW at 220 m, and KSS at 110 m (Mori et al. 2003).

We processed nearly 20 years of data covering the period from 2 March 2002 to 31 December 2023, although the starting date of analysis differs among the stations.

3.2 Method: Calculation of SBL

We analyzed the data using the SBL calculation method developed by Ichihara et al. (2023). While they used all three components of the seismometer data, we used only the vertical component, because the horizontal components sometimes had problems. A schematic diagram illustrating the calculation procedure is shown in Fig. 3. The detailed procedure is as follows.

Step1-1.

We calculated the power spectral densities (PSDs), $P_f(t, f)$, from the vertical seismograms at each station using a time window of 10.24 s sliding every 10 s. The variables *t* and *f* denote the central time of the window and the frequency, respectively. The calculation was restricted to the period between 18:00 of the previous day and 06:00 of the following day to avoid the influence of anthropogenic noise, which is predominant during daytime. The calculation of PSDs was performed on an hourly basis, and time periods with more than 30% missing data were excluded from the analysis because the data acquisition was unstable during those periods.

Step1-2.

We calculated the seismic power by integrating the PSDs over a limited frequency range. Ichihara et al. (2023) used the frequency band 3.5–7.0 Hz to include continuous volcanic signals and exclude characteristic noise associate with high precipitation at Kirishima volcano. We employed the same frequency band, which we validate later.

$$\text{Seismic Power:} \quad E(t) = \int_{3.5}^{7.0} P_f(t, f)\, df\,, \tag{1}$$

Step1-3.

The data were divided into two time windows: 18:00–24:00 of the previous day and

198 00:00–06:00 of the following day. For each time window, a representative value of the
199 seismic power was determined through statistical processing of the dataset. Specifically,
200 we adopted the lowest 20th percentile of the seismic power values. This percentile-
201 based approach is intended to suppress the influence of transient earthquakes, thereby
202 extracting weak volcanic signals. The square root of the representative seismic power
203 value was then defined as the SBL.

204 $$\text{Seismic background level: } SBL = \sqrt{E(t)}, \quad (2)$$

205 SBL values (raw SBL) were obtained two per day unless data are missing.

206 Step2.

207 A smoothing process was applied to exclude short-term fluctuations by selecting the
208 20th percentile of the raw SBL values within the previous seven days including the
209 current day (up to 14 samples). When fewer than 70% of the data (i.e. fewer than 10
210 samples) were available, the value for that day was excluded from the analysis. This
211 procedure effectively suppressed day-to-day variations related to weather conditions, as
212 shown in Fig. 3b, and yielded the final time series of SBL.

213 **3.3 Method: Calculation of normalized SBL ratio**

214 To identify differences in the temporal evolution of the SBL among observation sites,
215 we calculated the SBL ratios between station pairs. In this process, we first computed
216 the normalized SBL by dividing the smoothed SBL by its mean value over a reference
217 period, and then took the ratio between stations. For the reference period, we selected
218 December 2019 to January 2020, when the station with the longest continuous record
219 (KSHA) exhibited its highest SBL levels.

220 **3.4 Method: Calculation of SBL spectra**

221 We also calculated daily spectra to examine variations in the spectral components and to
222 obtain supplementary information on the onset and termination of weak signals.
223 Specifically, we stacked the power spectral densities of time windows corresponding to
224 the 5th to 20th percentiles of seismic power. Although Ichihara et al. (2023) normalized
225 the stacked spectra by the maximum value within 1–15 Hz, we used the maximum
226 within the 3.5-7.0 Hz band used for the SBL calculation. This approach was adopted to
227 focus on the spectral characteristics within the SBL calculation band.

228 **3.5 Method: Reclassification of earthquake types based on JMA catalog**

229 We reclassified the events into three groups: high-frequency (A- and BH-type), low-

frequency (BL-type), and harmonic/monochromatic (BP- and BT-type) earthquakes, where the type names follow the JMA classification (JMA 2024). A-type earthquakes are VT events, whereas B-type earthquakes are low-frequency events with unclear phase onsets. Among the B-type earthquakes, those with relatively high-frequency components are classified as BH-type, those with relatively low-frequency components as BL-type, those exhibiting harmonic oscillations as BP-type, and those with gradually decaying monochromatic tail as BT-type.

4. Results

4.1 Overview of temporal changes of SBL

4.1.1 SBL

Figure 4b shows the temporal changes in the SBL, whereas Fig. 4a shows the periods defined by focusing on the temporal evolution of the SBL at KSHA, which has the longest observation record. The specific periods and their characteristic trends are summarized in Table 1.

Although there are slight differences among the stations, they exhibit similar variation

246 trends. No obvious annual periodicity (seasonal variation) is observed. When multiple

247 stations are operated, their SBL variations are in general coherent.

248 **4.1.2 Normalized SBL ratio**

249 Figure 4c shows the normalized SBL ratios (see Section 3.3) since 2011, when station

250 KSAO was installed. For each station pair, we selected KSAO, the station farthest from

251 the Yugama crater, as the reference and compared the ratios of KSHA/KSAO and

252 KSW/KSAO. The normalized SBL ratio of KSHA/KSAO increased during the 2018

253 unrest, while it remained low during the 2014 unrest. In contrast, the normalized SBL

254 ratio of KSW/KSAO remained approximately constant (~1) throughout both unrest

255 periods. These temporal changes in the normalized SBL ratios are evident in the

256 logarithmic plots of SBL growth (Fig. 4b).

257 **4.2 Comparison with seismicity**

258 We compared the temporal variations in the SBL with seismic activity to investigate

259 their temporal correspondence and characteristic differences among the unrest episodes.

260 Figure 4d shows the monthly number of earthquakes since August 2002, mainly

261 occurring around the Yugama crater and Ainomine areas (JMA 2013).

4.2.1 Before 2014 unrest (Period I-IV)

During Period I, the SBL showed an increasing trend, whereas it decreased during Period II. During both periods, no notable change in seismic activity was observed. In Period III (2007), a slight increase in seismicity was observed, during which the SBL showed an increasing trend. In Period IV (2011), there were periods when the number of earthquakes exceeded that of the 2007 activity. The SBL remained at higher levels than those in the previous years, but no distinct increase in the SBL was observed.

4.2.2 2014 unrest (Period V-VI)

In Period V with the increasing SBL, an unrest has been reported with many volcanic earthquakes around the Yugama crater (Fig. 4b,d). The left column of Fig. 5 focuses on the 2014 unrest, which began in March 2014.

According to JMA (2014), small-amplitude volcanic earthquakes with shallow hypocenters beneath the Yugama crater started to increase around 16:00 on 6 March 2014. The activity became more intense in early May 2014 (Fig. 5g). The events were classified as high-frequency earthquakes (Fig. 5k). Subsequently, the SBL began to increase around May 2014 (Fig. 5a), slightly delayed relative to the onset of seismic

activity. In the SBL spectra, a spectral component around 3 Hz appeared in March 2014. In May 2014, the 3 Hz component became more pronounced, and another component around 4–5 Hz strengthened. Although the daily number of earthquakes decreased in July 2014, the SBL continued to increase. The SBL began to decline between July and September 2015, during which the seismic activity further decreased (Fig. 5a, g). Then the SBL continued to decrease until late 2016, at which time the spectral components around 3 Hz and 4–5 Hz disappeared (Fig. 5a, e).

4.2.3 2018 unrest (Period VII-IX)

A prolonged unrest occurred from 2018 to 2022. The right column of Fig. 5 focuses on the 2018 unrest. The SBL began to increase in late 2017, preceding the increase in seismic activity (Fig. 5b). Volcanic earthquakes increased in April 2018 (Fig. 5h). This increase was characterized by a sudden rise in activity and large amplitudes (Fig. 5j). The sharpness of this onset was particularly striking compared with that of the 2014 unrest. At the beginning of the activity, high-frequency earthquakes were dominant. Then, harmonic events became predominant (Fig. 5l).

In 2018, the SBLs at KSHA, KSE, and KSW showed synchronous fluctuations, which

were most pronounced at KSW (Fig. 5b). The SBL kept growing until early 2020, after which it remained at a high level. A component around 5–6 Hz appeared in late 2017, when the SBL started increasing, and became more pronounced in April 2018, when the seismic unrest started (Fig. 5f).

Around early 2022, when the number of earthquakes markedly decreased (Fig. 4d), the SBL began to show a slight decline (Fig. 4b).

4.3 Comparison with ground deformation

We compared the temporal variations in the SBL with ground deformation to examine their relationship and the depth dependence of the sources of activity.

Figure 4e shows the time series of baseline length changes between the GNSS stations G03 and G07, which are located on opposite sides of the Yugama crater (Fig. 2b). The baseline length is about 1,227 m, and such a local-scale baseline is generally sensitive to shallow deformation sources. Figure 4f presents the regional-scale areal strain calculated from three GEONET stations (Fig. 2a), which is instead sensitive to deeper crustal deformation sources. It should be noted that the areal strain calculation did not correct for the postseismic deformation following the 2011 Tohoku-Oki earthquake.

310 **4.3.1 Before 2014 unrest (Period I-IV)**

311 No obvious increase in areal strain corresponding to Period-I (2004–around April 2005)
312 or Period-III (around May 2007–2008) was observed (Fig. 4f). For Period IV (after
313 March 2011), volcanic-related deformation cannot be distinguished from the
314 postseismic deformation. Although the baseline length shows an overall trend of
315 contraction (Fig. 4e), the data sampling was insufficient during these periods, and
316 therefore the changes remain uncertain.

317 **4.3.2 2014 unrest (Period V-VI)**

318 The local extension started between the two data points in August 2012 and July 2014
319 (Fig. 4e). The SBL also began to increase in May 2014 (Period V). It turned to decrease
320 around May 2015 (Period VI), while the local extension seems to continue until the
321 measurement in May 2016. The subsequent baseline measurements (September 2016
322 and June 2017) show that the local deformation was in a contraction phase in the latter
323 half of Period-VI, when the SBL had returned to its pre-2014 level. The detailed
324 comparison between the SBL and the local deformation is limited because of the sparse
325 sampling interval, which we discuss in Section 5.1.1.

The areal strain began to increase in early 2014 (Fig. 4f), preceding the increase in the SBL from around May 2014 (Period V). The increase in areal strain slowed down around February 2015, and the areal strain began to decrease around November 2015. Coherently, the SBL started to decline around the boundary between Periods V and IV.

4.3.3 2018 unrest (Period VII-IX)

The local extension data in May 2018 showed an extension compared with the previous measurements around the boundary between VI and VII (Fig. 4e), indicating that the preceding contraction trend had at least weakened. The SBL had already started growing. The baseline length turned to a contraction trend in 2022, while the SBL slightly decreased around early 2022 (Period IX) and stabilized in Period X (Fig. 4b). The areal strain (Fig. 4f) began to increase in late 2017 (around the boundary between Periods VI and VII), around which the SBL showed a slight upward trend. In Period IX when the SBL slightly decreased, the increasing trend in areal strain became less obvious.

5. Discussion

342 **5.1 Relationship between SBL and volcanic activity**

343 Table 2 summarizes the sequences presented in Section 4. Here we assume that the

344 GNSS observations of the local extension (Fig. 4e) and the areal strain (Fig. 4f)

345 represent the shallow and deep deformations, respectively (see Appendix A). We

346 combine the results in Table 2 and other observations to infer the relevant volcanic

347 activity.

348 **5.1.1 2014 and 2018 unrest**

349 We identified two common features. First, the SBL increases before or during the

350 enhanced volcanic seismic activity. Second, the SBL tends to increase during the

351 inflation phases of both deep and shallow deformation sources, and to decrease when

352 the inflating trend slows down, stagnates, or reverses.

353 Terada et al. (2025) reported the tiltmeter observations around the Yugama crater (at

354 KSE, KSS, and KSW), which complement the sparse GNSS data of the local extension.

355 They recorded two distinct deformation phases. From 3 March 2014, all stations exhibit

356 northwest-up tilts, indicating a deep source. From 14 March 2014 to October 2015, a

357 radial pattern of uplifts indicated an inflation at a shallow source around Yugama. A

358 comparison between the tiltmeter observations and the SBL variations suggests that the
359 SBL began to decrease during the period when the uplift around Yugama continued.
360 Knowing that the ground deformations are of volcanic origin (Munekane 2021; Terada
361 et al. 2025), we interpret the observed relationship between the SBL and the
362 deformation of the deep and shallow sources as indicative of the supply of volcanic
363 fluids from deeper to shallower regions within the volcanic system.

364 **5.1.2 Before 2014 unrest**

365 SBL variations were also observed in Periods I−III without significant volcanic unrest.
366 Terada and Kuwahara (2025) reported the daily mean temperature of the Yugama crater
367 lake and showed that the lake water temperature has never fallen below 0 °C even
368 during winter since 2009, including both unrest and non-unrest periods. This
369 observation suggests the continuous presence of a heat contribution to the shallow
370 region beneath Yugama, either through the direct supply of volcanic fluids or through
371 thermal input not directly associated with the fluids themselves. Therefore, it is
372 reasonable to consider that volcanic vibration signals have been present throughout the
373 entire period after Period-I.

In Period-I, a water jet and a color change of the lake surface were observed at Yugama on 17 May 2004 (Volcanic Fluid Research Center, Tokyo Institute of Technology 2004; JMA 2013). In Period-II, no notable surface phenomena were reported, while the SBL showed a decreasing trend. In Period-III, the number of volcanic earthquakes slightly increased, and the appearance of new fumaroles around Yugama was reported (JMA 2008a, b, 2013). No inflation of the deep deformation source was detected during these periods.

Although shallow deformation was not clearly resolved, geomagnetic measurements indicated an increase in rock magnetization beneath the Yugama crater lake, interpreted as the thermomagnetic effect associated with progressive cooling of the subsurface (Takahashi and Fujii 2014). This cooling trend is consistent with the reduced upward flux of hydrothermal fluids from the depth after 1992. In addition, chemical analyses of the lake water revealed that the system was in a self-sealing stage, during which the development of the self-sealing zone suppressed the supply of magmatic fluids from the deeper part of the system (Yaguchi et al. 2021). The increase in SBL observed during these periods may represent a minor fluctuation in volcanic activity occurring in the

shallow depth beneath Yugama, within an overall declining and cooling trend of the hydrothermal system.

5.2 Location of the SBL vibrations source

As a preliminary step towards understanding the mechanism of SBL vibrations, we attempted to estimate their source locations.

5.2.1 Polarization analysis

Hirose and Ueda (2025) analyzed the location of continuous tremor observed at Kirishima Volcano using the three-component data from a single seismometer about 2 km from the active crater. They estimated the back azimuths of the signals by applying Rayleigh-wave-based polarization analysis, and subsequently combined the results from multiple stations to infer the source location.

We conducted a polarization analysis on the SBL vibrations, following the method of Hirose and Ueda (2025) (see Appendix B). The analysis targeted the period from December 2019 to January 2020, when the SBL level was relatively high. The joint probability distribution obtained from the combined analysis of KSHA, KSE, KSW, and KSS showed a very high probability around the Yugama crater (Fig. 6a). The horizontal

406 distance between the seismometers and the estimated vibration source was less than
407 approximately 1 km away. If Rayleigh waves are observed at such short distances, the
408 source should be shallow.

409 **5.2.2 A slight difference of the location of SBL vibrations and causes of normalized**
410 **SBL ratio changes**

411 We found that the horizontal location of the SBL vibration source estimated in Section
412 5.2.1 was near the Yugama crater. This region is close to the hypocenters of high-
413 frequency earthquakes observed during the same period (Fig. 6b). We therefore focused
414 on the hypocenters of high-frequency earthquakes associated with the 2014 and 2018
415 unrests. As shown in Fig. 6c and 6d, the hypocenters during the 2018 unrest were
416 located slightly to the northeast compared with those during the 2014 unrest, that is, in
417 the direction closer to KSHA and KSE. Consistently, Terada et al. (2025) showed that
418 the deformation source inferred from tiltmeter data during the 2018 unrest was located
419 further to the northeast than that during the 2014 unrest.

420 To examine vertical differences in the SBL vibration source location, we focused on
421 contrasts in earthquake types between the 2014 and 2018 unrests. The 2018 unrest was

422 characterized by the occurrence of many harmonic earthquakes (Table 2). Sources of
423 the same type observed during 1992–1993 were reported to be located at a depth of
424 approximately 200 m directly beneath the Yugama crater lake (Kumagai et al., 2002b).
425 This suggests that, compared with the 2014 unrest, the 2018 unrest involved a larger
426 proportion of earthquakes with shallower hypocenters. We infer that the 2018 unrest
427 affected shallower portions of the hydrothermal system. This interpretation is consistent
428 with Kanda et al. (2025). They estimated the locations of thermal demagnetization
429 sources beneath the Yugama area for May 2014 (the 2014 unrest) and for the period
430 from April 2018 to July 2021 (the 2018 unrest), and reported that the source depths
431 during the 2018 unrest were shallower than those during the 2014 unrest.
432 Although the source locations of SBL vibrations do not necessarily coincide with those
433 of hypocenters or thermal demagnetization sources, we may explain the observed
434 temporal variations in the normalized SBL ratios (Section 4.1.2) by a northeastward and
435 upward shift of its source location. Namely, the activity center during the 2018 unrest
436 was likely closer to stations KSE and KSHA than during the 2014 unrest. The relative
437 values of the SBL ratio can thus provide spatial information about the source location.

438 At the same time, caution is required when comparing absolute SBL values at the same
439 station across different periods, because they do not necessarily represent the level of
440 volcanic activity but the relative distances of the source. Indeed, the SBL amplitudes at
441 KSHA and KSE were larger during the 2018 unrest than during the 2014 unrest,
442 whereas at KSW, KSS, and KSAO, the SBL amplitudes were larger during the 2014
443 unrest.

444 **5.3 Possible mechanism of the SBL vibrations**

445 We consider it more reasonable to assume a non-destructive mechanism for the SBL
446 vibration source, because the vibrations persist continuously over long periods. In
447 volcanic regions, one possible continuous vibration source is tremor associated with
448 fumarolic activity. A geothermal zone developed on the northern outer slope of the
449 Yugama crater rim, where fumaroles are present (Ohba and Yaguchi 2025). However,
450 based on the results presented in Section 5.2.1, the estimated SBL source location
451 differs from this fumarolic area, and this mechanism is therefore considered unlikely.
452 Instead, we propose that the SBL vibrations are related to non-destructive processes
453 within a shallow hydrothermal system. Jolly et al. (2020) suggested that persistent

tremor observed at Whakaari (White Island) may be generated by frothing within a hydrothermal system. Ichihara et al. (2023) proposed that the SBL vibrations may involve similar processes.

Around the Yugama crater, a well-developed hydrothermal system and shallow groundwater aquifers are present (Hirabayashi 1999; Terada 2018). We suggest that the supply of volcanic fluids—whether magma itself or volcanic gases separated from it—to the shallower region beneath Yugama heated these subsurface systems, thereby generating the vibrations. Because the SBL source is inferred to be located in a very shallow region directly beneath the Yugama crater (Section 5.2.1), conditions allowing the coexistence of gas and liquid phases are plausible (Kumagai et al. 2002a; Taguchi et al. 2018). Therefore, this mechanism represents one plausible explanation for the observed SBL vibrations.

In this study, a quantitative estimation of the source depth has not yet been achieved. Constraining the depth of the vibration source would enable the comparison with the subsurface structure derived from magnetotelluric (MT) soundings (Matsunaga and Kanda 2025) and would contribute to a more detailed understanding of the vibration

mechanism.

6. Conclusion

In this study, we applied a statistical approach to long-term seismic observations around the Yugama crater at Kusatsu-Shirane volcano and clarified temporal variations in the SBL. The analysis of nearly 20 years of data revealed that the SBL increased during the unrest episodes in 2014 and 2018, showing good correlation with both deep and shallow sources of ground deformation. This result is interpreted as reflecting changes in volcanic activity driven by the supply of volcanic fluids. The variation in normalized SBL ratios between the two unrest episodes further suggests slight differences in the activity center.

Overall, the results demonstrate that SBL analysis is a powerful tool for monitoring volcanic activity. In particular, the SBL can reveal subtle variations in the state of the hydrothermal system, even during non-unrest periods. When combined with SBL ratio analysis, it also provides spatial information on the vibration source.

Appendix A: Ground deformation

A1. ground deformation by volcanic activity of Kusatsu-Shirane, Yugama area

Two major sources of ground deformation have been reported to be associated with the volcanic activity around the Yugama crater of Kusatsu-Shirane volcano.

Shallow source beneath Yugama crater lake

JMA (2016) reported the presence of an inflation source located in the very shallow region directly beneath the Yugama crater (at an elevation of approximately 1660 m), based on the results of GNSS campaign observations conducted in July and November 2014. The GNSS stations used for the baseline length changes shown in Fig. 4e are the same as those used in that report. Therefore, we infer that the baseline length changes in Fig. 4e reflect the inflation of the shallow deformation source beneath Yugama.

Similarly, an analysis of tiltmeter data around Yugama also revealed a shallow deformation source beneath the crater (Terada et al. 2025).

Deep source at approximately 2km northwest from the Yugama area

Munekane (2021) analyzed GEONET data and identified a deformation source located approximately 2 km northwest of the Yugama crater at a depth of about 4 km.

According to that study, the Kusatsu-Shirane source was generally inflating after 2013, with distinct inflation episodes from late 2013 to 2015 and again from late 2017 onward, which corresponded to the periods of volcanic unrest around Yugama in 2014 and 2018, respectively.

Munekane (2021) reported results only for the period from 2013 to 2020 and therefore did not cover the full duration of our SBL analysis. To examine longer-term changes, we calculated the areal strain for the GNSS stations shown in Fig. 2a using the GEONET F5 provided by the Geospatial Information Authority of Japan (Takamatsu et al. 2023). To reduce short-term fluctuations, a 30-day moving average was applied. Seasonal variations were extracted from the stable period of 2008–2010 and removed from the entire dataset using the obtained seasonal component. The resulting areal strain was compared with that estimated from the volume change reported by (Munekane 2021). For simplicity, we fixed the latitude, longitude, and depth of the deformation source and used the elevation-modified Mogi model (Fukui 2008). Although the amplitude of the changes in 2014 differed slightly between the two datasets, their temporal trends were consistent, and both the amplitude and the trend showed good

agreement after 2015. Therefore, we assumed that the areal strain reflects the behavior of the deep deformation source throughout the analysis period.

Appendix B: Polarization analysis of SBL vibrations

B1. Method

This analysis is based on the polarization analysis approach developed by Hirose and Ueda (2025), which extends the method of Meza-Fajardo et al. (2015). Our approach differs from that of Hirose and Ueda (2025) in the way back azimuths are determined, and also in that Kernel Density Estimation (KDE) is employed for estimating the directional distribution. The following sections describe the computational procedure, as well as the definitions of the probability density estimation and the joint probability used in this study. For detailed derivations of back-azimuth estimation for each frequency in each time window, the reader is referred to Hirose and Ueda (2025).

Step1:

The polarization analysis was performed for waveform data within a 10.24-s time window using the method of Hirose and Ueda (2025). The analysis was applied to time

534 windows where the Seismic Power percentile was between the 20th and 40th. After

535 applying the NIP filter, the back azimuth corresponding to the frequency with the

536 largest mean amplitude within the 3.5–7.0 Hz band was adopted as the back azimuth for

537 that time window.

538 Step2:

539 We estimated the density distribution of the back-azimuth dataset for each day using a

540 non-parametric method.

541 $$\hat{f}(\theta; h) = \frac{1}{n}\sum_{i=1}^{n} K_h(\theta - \theta_i) \qquad (B.1)$$

542 where, $K_h = K(\theta/h)/h$ is kernel function, and *h* is smoothing parameter (Taylor

543 2008). We used the von Mises distribution (Mardia and Jupp 2010) as the kernel.

544 $$K(\theta; \mu, \kappa) = \frac{1}{2\pi I_0(\kappa)} e^{\kappa \cos(\theta - \mu)} \qquad (B.2)$$

545 where, I_0 is the modified Bessel function of order 0. κ is concentration parameter and

546 is the reciprocal of *h*. From Equations (B.1) and (B.2), the kernel density estimation

547 using the von Mises distribution as the kernel is given by:

548 $$\hat{f}(\theta; \kappa) = \frac{1}{n(2\pi)I_0(\kappa)}\sum_{i=1}^{n} exp\{\kappa \cos(\theta - \theta_i)\} \qquad (B.3)$$

549 In this study, we compared the estimated density distribution with the observed

550 frequency distribution and adopted $\kappa = 50$, which showed a good agreement between

551 the two. The half width at half maximum (HWHM) in this case is approximately 9.6°.

552 The grid interval (θ_i spacing) used for summing the kernel functions was set to 0.5°. In

553 addition, datasets with fewer than 100 samples were excluded from the analysis.

554 Step3:

555 The probability density distributions estimated for each day were averaged over the

556 analysis period, and the resulting mean distribution was regarded as the probability

557 density distribution for that period.

558 Step4:

559 We applied the cross-bearings approach (Lehr et al. 2019; Hirose and Ueda 2025) to the

560 probability density distributions of back azimuths estimated at each of the four

561 observation sites to estimate the vibration source location. Specifically, the probability

562 density distributions obtained in Step 3 were back-projected onto the grid. The joint

563 probability of the intersecting beams is given by:

564 $$p(x_j, y_j) = \frac{\prod_i^M f_i(\phi_{ij})}{\sum_{i=1}^N (\prod_i^M f_i(\phi_{ij}))} \qquad (B.4)$$

565 where ϕ_{ij} is the back azimuth at *i*-th station for a signal starting at a *j*-th search grid

which location is (x_j, y_j). The grid covers the area from 36.62°N to 36.66°N in latitude and from 138.51°E to 138.56°E in longitude, with a spacing of 0.001° in both directions.

B2. Result

Figure B2 shows the probability distributions obtained by back-projecting the directional density distributions from each station onto the grid, together with the joint probability obtained by combining the results from multiple stations. The probability is high around the Yugama crater.

List of abbreviations

GEONET: GNSS Earth Observation Network System

GNSS: Continuous global navigation satellite system

GSI: Geospatial Information Authority of Japan

HWHM: the half width at half maximum

JMA: Japan Meteorological Agency

KDE: Kernel Density Estimation

SBL: Seismic background level

VLP earthquake: very-long-period earthquake

VT earthquake: volcano-tectonic earthquake

Declarations

Ethics approval and consent to participate

Not applicable.

Consent for publication

Not applicable.

Availability of data and materials

Continuous seismic waveform data used in this study were obtained from the Japan Meteorological Agency and Tokyo Institute of Technology (reorganized as the Institute of Science Tokyo in October 2024) through institutional access. The seismic data and GNSS campaign observation data were accessed through institutional access. Access to these data is subject to the data policies of the respective institutions. GNSS GEONET data are publicly available from the Geospatial Information Authority of Japan (GSI). The smoothed SBL datasets provided as Supplementary Information.

Competing interests

The authors declare that they have no competing interests.

Funding

This study was supported by the Ministry of Education, Culture, Sports, Science, and Technology of Japan (MEXT) under the third Earthquake and Volcano Hazards Observation and Research Program (Earthquake and Volcano Hazard Reduction Research).

Authors' contributions

TK and MI drafted the manuscript. TK and YY prepared the SBL data. TK performed the data analysis. TK, AK, and KN contributed to the interpretation. All authors discussed the results and contributed to the final manuscript.

Acknowledgements

We thank the Geospatial Information Authority of Japan (GSI) for providing GNSS data from GEONET (GNSS Earth Observation Network System; https://terras.gsi.go.jp/). We also thank Hiroshi Munekane for providing the analysis results of volume changes at Kusatsu-Shirane volcano. We thank the editor (XXXX) and the reviewers (YYYY and one anonymous reviewer) for their constructive comments that helped improve this manuscript.

Authors' information

620 Authors and Affiliations

621 Japan Meteorological Agency

622 Present address: Hot Springs Research Institute of Kanagawa Prefecture, 586 Iriuda,

623 Odawara, Kanagawa, Japan

624 Tsukasa Kobayashi

625 The Earthquake Research Institute, The University of Tokyo, Tokyo, 113-0032, Japan

626 Mie Ichihara & Yohei Yukutake

627 Volcano and Earthquake Research Division, Multidisciplinary Resilience Research

628 Center, Institute of Integrated Research, Institute of Science Tokyo, 2-12-1 Ookayama,

629 Meguro, Tokyo, 152-8551, Japan

630 Akihiko Terada

631 Multidisciplinary Resilience Research Center (Kusatsu-Shirane Volcano Observatory),

632 Institute of Integrated Research, Institute of Science Tokyo, Gunma, Japan

633 Kenji Nogami

634

635 **References**

636 Acocella V, Ripepe M, Rivalta E, et al (2024) Towards scientific forecasting of magmatic

637 eruptions. Nat Rev Earth Environ 5:5–22. https://doi.org/10.1038/s43017-023-
638 00492-z

639 Behr Y, Christophersen A, Miller C (2025) Probabilistic, Multi-Sensor Eruption
640 Forecasting. Geophysical Research Letters 52:e2024GL112029.
641 https://doi.org/10.1029/2024GL112029

642 Burchardt S, Annen CJ, Kavanagh JL, Hilmi Hazim S (2022) Developments in the study
643 of volcanic and igneous plumbing systems: outstanding problems and new
644 opportunities. Bull Volcanol 84:59. https://doi.org/10.1007/s00445-022-01564-6

645 Fukui K (2008) Studies on Evaluation Method of Volcanic Activity. TECHNICAL
646 REPORTS OF THE METEOROLOGICAL RESEARCH INSTITUTE 105–122.
647 https://www.mri-
648 jma.go.jp/Publish/Technical/DATA/VOL_53/tec_rep_mri_53_141.pdf. Accessed
649 2 Nov 2025 (in Japanese)

650 Hirabayashi J (1999) Formation of Volcanic Fluid Reservoir and Volcanic Activity.
651 Journal of Hot Spring Sciences 79:99–105 (in Japanese with English abstract)

652 Hirose T, Ueda H (2025) Seismic Wavefield Change Preceding the Eruption of Shinmoe-
653 Dake, Kirishima Volcano, Japan, Inferred From Polarization Analysis. Journal of
654 Geophysical Research: Solid Earth 130:e2024JB029358.
655 https://doi.org/10.1029/2024JB029358

656 Ichihara M, Ohminato T, Konstantinou KI, et al (2023) Seismic background level (SBL)
657 growth can reveal slowly developing long-term eruption precursors. Sci Rep
658 13:5954. https://doi.org/10.1038/s41598-023-32875-z

659 Ida Y, Osada N, Sawada M, et al (1989) Seismological Study Based on Recently Installed
660 Permanent Stations and a Small Eruptive Event on January 6, 1989 at Kusatsu-
661 Shirane Volcano. Bulletin of the Earthquake Research Institute, University of
662 Tokyo 64:325–345. https://doi.org/10.15083/0000032805 (in Japanese with
663 English abstract)

664 Ishizaki Y, Kametani N, Numata W (2025) Geology and Eruptive History of Kusatsu-

Shirane Volcano. In: Ohba T, Terada A (eds) Kusatsu-Shirane Volcano. Springer Nature Switzerland, Cham, pp 1–20

Japan Meteorological Agency (2018a) Volcanic Activity of Kusatsu-Shiranesan Volcano (February 2018 - May 2018). Report of the Coordinating Committee for Prediction of Volcanic Eruption https://www.jma.go.jp/jma/kishou/shingikai/ccpve/Report/130/kaiho_130_09.pdf. Accessed 25 Oct 2025 (in Japanese)

Japan Meteorological Agency (2018b) Volcanic Activity of Kusatsu-Shiranesan Volcano (June - September, 2018). Report of the Coordinating Committee for Prediction of Volcanic Eruption https://www.jma.go.jp/jma/kishou/shingikai/ccpve/Report/131/kaiho_131_12.pdf. Accessed 25 Oct 2025 (in Japanese)

Japan Meteorological Agency (2018c) Volcanic activities of Kusatsu-Shiranesan during June., 2018. https://www.data.jma.go.jp/vois/data/report/monthly_v-act_doc/tokyo/18m06/305_18m06.pdf. Accessed 26 Dec 2025 (in Japanese)

Japan Meteorological Agency (2013) National catalog of the active volcanoes in Japan, 4th edn. https://www.data.jma.go.jp/svd/vois/data/tokyo/STOCK/souran_eng/menu.htm. Accessed 25 Oct 2025 (English version)

Japan Meteorological Agency (2008a) Volcanic activities of Kusatsu-Shiranesan during Jul., 2008. https://www.data.jma.go.jp/vois/data/report/monthly_v-act_doc/tokyo/08m07/305_08m07.pdf. Accessed 26 Oct 2025 (in Japanese)

Japan Meteorological Agency (2008b) Volcanic activities of Kusatsu-Shiranesan during Oct., 2008. https://www.data.jma.go.jp/vois/data/report/monthly_v-act_doc/tokyo/08m10/305_08m10.pdf. Accessed 26 Oct 2025 (in Japanese)

Japan Meteorological Agency (2024) Seismic observation data file format. In: Japan Meteorological Agency. https://www.data.jma.go.jp/vois/data/filing/bulletin/data/format/vtrfmt_j.html.

693 Accessed 25 Nov 2025 (in Japanese)

694 Japan Meteorological Agency (2014) Volcanic activities of Kusatsu-Shiranesan during
695 Mar., 2014. https://www.data.jma.go.jp/vois/data/report/monthly_v-
696 act_doc/tokyo/14m03/305_14m03.pdf. Accessed 1 Nov 2025 (in Japanese)

697 Japan Meteorological Agency (2016) Volcanic Activity of Kusatsu-Shiranesan Volcano
698 (October 2014 –February 23, 2015). In: Report of the Coordinating Committee
699 for Prediction of Volcanic Eruption.
700 https://www.jma.go.jp/jma/kishou/shingikai/ccpve/Report/120/kaiho_120_06.pd
701 f. Accessed 1 Nov 2025 (in Japanese)

702 Jolly A, Caudron C, Girona T, et al (2020) 'Silent' Dome Emplacement into a Wet
703 Volcano: Observations from an Effusive Eruption at White Island (Whakaari),
704 New Zealand in Late 2012. Geosciences 10:142.
705 https://doi.org/10.3390/geosciences10040142

706 Kametani N, Yoshimoto M, Ishimine Y, Honda R (2025) Eruption Products and Damage
707 Caused by the 2018 Phreatic Eruption of Mount Motoshirane. In: Ohba T, Terada
708 A (eds) Kusatsu-Shirane Volcano. Springer Nature Switzerland, Cham, pp 21–39

709 Kanda W, Koyama T, Matsunaga Y (2025) Geomagnetic Observations at Kusatsu-Shirane
710 Volcano. In: Ohba T, Terada A (eds) Kusatsu-Shirane Volcano. Springer Nature
711 Switzerland, Cham, pp 211–229

712 Kobayashi T, Kato K, Kawaguchi R, et al (2019) Report of Volcanic Activity at Kusatsu-
713 Shiranesan(Yugama Area), Japan in 2018-2019. AGU. https://agu-
714 do03.confex.com/agu/fm19/meetingapp.cgi/Paper/534577 Accessed 30 Sep 2025

715 Kumagai H, Chouet BA, Nakano M (2002a) Temporal evolution of a hydrothermal
716 system in Kusatsu-Shirane Volcano, Japan, inferred from the complex frequencies
717 of long-period events. Journal of Geophysical Research: Solid Earth 107:ESE 9-
718 1-ESE 9-10. https://doi.org/10.1029/2001JB000653

719 Kumagai H, Chouet BA, Nakano M (2002b) Waveform inversion of oscillatory signatures
720 in long-period events beneath volcanoes. https://doi.org/10.1029/2001JB001704

721 Kurihara R (2023) Temporal change of noise amplitudes observed in the stations of
722 Owakudani, Komagatake, Owakudani-Jizoson and Omatazawa. Report of the Hot
723 Springs Research Institute of Kanagawa Prefecture 55:35–43

724 Lehr J, Eckel F, Thorwart M, Rabbel W (2019) Low-Frequency Seismicity at Villarrica
725 Volcano: Source Location and Seismic Velocities. JGR Solid Earth 124:11505–
726 11530. https://doi.org/10.1029/2018JB017023

727 Mardia KV, Jupp PE (eds) (2010) Directional statistics. J. Wiley, Chichester New York

728 Matsunaga Y, Kanda W (2025) Magnetotelluric Imaging of the Magmatic–Hydrothermal
729 System of Kusatsu–Shirane Volcano. In: Ohba T, Terada A (eds) Kusatsu-Shirane
730 Volcano. Springer Nature Switzerland, Cham, pp 185–210

731 Matsunaga Y, Kanda W, Takakura S, et al (2020a) 3-D resistivity structure model around
732 Kusatsu-Shirane Volcano revealed by broadband magnetotellurics. pp V004-0018

733 Matsunaga Y, Kanda W, Takakura S, et al (2020b) Magmatic hydrothermal system
734 inferred from the resistivity structure of Kusatsu-Shirane Volcano. Journal of
735 Volcanology and Geothermal Research 390:106742.
736 https://doi.org/10.1016/j.jvolgeores.2019.106742

737 Meza-Fajardo KC, Papageorgiou AS, Semblat J-F (2015) Identification and Extraction of
738 Surface Waves from Three-Component Seismograms Based on the Normalized
739 Inner Product. Bulletin of the Seismological Society of America 105:210–229.
740 https://doi.org/10.1785/0120140012

741 Mori T, Hirabayashi J, Nogami K, Onizawa S (2003) Construction and application of
742 observation system in Kusatsu-Shirane volcano.

743 Munekane H (2021) Modeling long-term volcanic deformation at Kusatsu-Shirane and
744 Asama volcanoes, Japan, using the GNSS coordinate time series. Earth, Planets
745 and Space 73:192. https://doi.org/10.1186/s40623-021-01512-2

746 Niu J, Song T-RA (2020) Real-time and in-situ assessment of conduit permeability
747 through diverse long-period tremors beneath Aso volcano, Japan. Journal of

748 Volcanology and Geothermal Research 401:106964.
749 https://doi.org/10.1016/j.jvolgeores.2020.106964

750 Ohba T, Yaguchi M (2025) Volcanic Activity Cycles of the Kusatsu-Shirane Volcano,
751 Japan Revealed by the Geochemical Monitoring of Lake Water in the Yugama
752 Crater and Adjacent Fumarolic Gases. In: Ohba T, Terada A (eds) Kusatsu-Shirane
753 Volcano. Springer Nature Switzerland, Cham, pp 41–59

754 Poland MP, Anderson KR (2020) Partly Cloudy With a Chance of Lava Flows:
755 Forecasting Volcanic Eruptions in the Twenty-First Century. Journal of
756 Geophysical Research: Solid Earth 125:e2018JB016974.
757 https://doi.org/10.1029/2018JB016974

758 Stix J, De Moor JM (2018) Understanding and forecasting phreatic eruptions driven by
759 magmatic degassing. Earth Planets Space 70:83. https://doi.org/10.1186/s40623-
760 018-0855-z

761 Stix J, de Moor JM, Aiuppa A (2025) Understanding and forecasting sudden explosive
762 eruptions. Bull Volcanol 87:99. https://doi.org/10.1007/s00445-025-01886-1

763 Taguchi K, Kumagai H, Maeda Y, Torres R (2018) Source Properties and Triggering
764 Processes of Long-Period Events Beneath Volcanoes Inferred From an Analytical
765 Formula for Crack Resonance Frequencies. Journal of Geophysical Research:
766 Solid Earth 123:7550–7565. https://doi.org/10.1029/2018JB015866

767 Takahashi K, Fujii I (2014) Long-term thermal activity revealed by magnetic
768 measurements at Kusatsu-Shirane volcano, Japan. Journal of Volcanology and
769 Geothermal Research 285:180–194.
770 https://doi.org/10.1016/j.jvolgeores.2014.08.014

771 Takamatsu N, Muramatsu H, Abe S, et al (2023) New GEONET analysis strategy at GSI:
772 daily coordinates of over 1300 GNSS CORS in Japan throughout the last quarter
773 century. Earth, Planets and Space 75:49. https://doi.org/10.1186/s40623-023-
774 01787-7

775 Takeo M, Aoki Y, Koyama T (2022) Recent volcanic activity at the Asama volcano and

776 long-period seismic signals. Proceedings of the Japan Academy, Series B 98:416–
777 438. https://doi.org/10.2183/pjab.98.022

778 Taylor CC (2008) Automatic bandwidth selection for circular density estimation.
779 Computational Statistics & Data Analysis 52:3493–3500.
780 https://doi.org/10.1016/j.csda.2007.11.003

781 Terada A (2018) Kusatsu-Shirane volcano as a site of phreatic eruptions. Jour Geol Soc
782 Japan 124:251–270. https://doi.org/10.5575/geosoc.2017.0060 (in Japanese with
783 English abstract)

784 Terada A, Aoyama H, Yamada T, Yamamoto M (2025) Geophysical Observations of
785 Kusatsu–Shirane Volcano: Conceptual Model of the Hydrothermal System as a
786 Site of Phreatic Eruptions. In: Ohba T, Terada A (eds) Kusatsu-Shirane Volcano.
787 Springer Nature Switzerland, Cham, pp 159–184

788 Terada A, Kanda W, Ogawa Y, et al (2021) The 2018 phreatic eruption at Mt. Motoshirane
789 of Kusatsu–Shirane volcano, Japan: eruption and intrusion of hydrothermal fluid
790 observed by a borehole tiltmeter network. Earth Planets Space 73:157.
791 https://doi.org/10.1186/s40623-021-01475-4

792 Terada A, Kuwahara T (2025) Yugama Crater Lake: A Sensitive Window into the
793 Magmatic–Hydrothermal System of Kusatsu-Shirane Volcano. In: Ohba T, Terada
794 A (eds) Kusatsu-Shirane Volcano. Springer Nature Switzerland, Cham, pp 61–81

795 Volcanic Fluid Research Center, Tokyo Institute of Technology (2004) Recent activity of
796 Kusatsu-Shirane volcano -Water jet from crater lake Yugama on 17, May 2004-.
797 Bulletin of the Coordinating Committee for the Prediction of Volcanic Eruptions
798 49–54

799 Yaguchi M, Ohba T, Terada A (2021) Groundwater Interacting at Depth With Hot Plastic
800 Magma Triggers Phreatic Eruptions at Yugama Crater Lake of Kusatsu-Shirane
801 Volcano (Japan). Front Earth Sci 9:. https://doi.org/10.3389/feart.2021.741742

802 Yamasato H (2005) Modern History of Volcano Observation in Japan Especially Volcano
803 Surveillance of Japan Meteorological Agency. Bulletin of the Volcanological

804 Society of Japan 50:S7–S18. https://doi.org/10.18940/kazan.50.Special_S7

805

806

807 Caption

808 Table 1

809 Period defined from SBL at KSHA.

810 [footnote]

811 * The decrease in Period IX can be more clearly recognized when the results from KSE

812 are also taken into account.

813 ** Dates in parentheses correspond to the time intervals used for color coding in Fig. 4.

814

815

816 Table 2

817 Summary of characteristic differences in the SBL, seismicity, and ground deformation.

818

819

820 Figure 1

821 Location of Kusatsu, and seismicity and volcanic surface phenomena near the Yugama

822 crater.

(a) Location of Kusatsu and Yugama.

(b) Monthly number of earthquakes and volcanic surface phenomena near the Yugama crater.

Black bars show the monthly number of earthquakes counted by JMA.

Gray dashed line indicates the change in earthquake-counting rules.

Red triangles indicate eruptions.

Blue triangles indicate color changes of the Yugama crater lake and water jets.

Orange squares indicate the appearance of new fumaroles near Yugama.

Figure 2

Locations of observation sites and sources of ground deformation.

(a) Regional map. The dashed square shows the area shown in panel (b).

(b) Local map around the Yugama crater.

Squares indicate seismometers. Filled symbols are installed by the JMA, and open symbols by the Institute of Science Tokyo.

839 Circles indicate GNSS stations. Filled symbols are installed by JMA, and open symbols

840 by the Geospatial Information Authority of Japan (GSI).

841 Plus sign indicates deep source of ground deformation reported by Munekane (2021).

842 Cross indicates the near-Yugama source of ground deformation reported by JMA

843 (2015).

844

845 Figure 3

846 Schematic illustration of the calculation method for the Seismic background level

847 (SBL).

848 (a) Daily calculation of raw SBL (example: site KSAO, vertical component).

849 (b) Calculation of time series of smoothed SBL.

850

851

852 Figure 4

853 Long-term variations in the SBL, seismicity, and ground deformation (shallow and

854 deep).

855 (a) Periods listed in Table 1 and volcanic surface phenomena. The symbols are the same

856 as in Figure 1b.

857 (b) SBL at sites around the Yugama crater (KSE, KSHA, KSS, KSW, KSAO).

858 (c) Normalized SBL ratio. The reference period for normalization is December 2019 to

859 January 2020. Green shows KSHA/KSAO. Pink shows KSW/KSAO.

860 (d) Seismicity (monthly number of high-frequency, low-frequency, and harmonic and

861 monochromatic events). Data shown is from August 2002 onwards.

862 (e) GNSS baseline length change, mainly reflecting deformation of the shallow source.

863 Red symbols indicate results from GNSS campaign observations, and blue symbols

864 indicate continuous GNSS data (observations suspended during the snowy season).

865 (f) GNSS areal strain, mainly reflecting deformation of the deep source. Black dots

866 show the raw areal strain calculated from GEONET, and the red line shows the strain

867 after smoothing and removing the seasonal trend. Blue dots show volume change

868 reported by Munekane (2021). The dashed line indicates the date of the Tohoku–Pacific

869 Ocean earthquake on March 11, 2011. The deformation drawn by gray background

870 color immediately after the event was due to postseismic deformation.

Figure 5

Comparison of the onset of volcanic unrest in 2014 and 2018.

(a, b) SBL at sites around the Yugama crater (KSE, KSHA, KSS, KSW, KSAO). Left blue dashed line in panel (a) indicates March 6, 2014. Right blue dashed line in panel (a) indicates May 1, 2014. Blue dashed line in panel (b) indicates April 21, 2018. The same goes for the following panels.

(c, d) Normalized SBL ratio. Green shows KSHA/KSAO. Pink shows KSW/KSAO.

(e, f) Daily SBL spectra at KSHA.

(g, h) Seismicity (daily number of earthquakes).

(i, j) Seismicity (maximum amplitudes of earthquakes). In the 2018 unrest graph, the dashed line shows all earthquakes, whereas the solid line excludes the earthquake that occurred at 18:10 on April 30, 2018. This earthquake was the largest event since 2014 (JMA, 2018) and had a magnitude of 0.6 (JMA catalog).

(k, l) Monthly ratio of volcanic earthquake types. Red indicates high-frequency

887 earthquakes, green indicates low-frequency earthquakes, and blue indicates harmonic
888 and monochromatic earthquakes.
889
890
891 Figure 6
892 Location of the SBL vibration source estimated by polarization analysis and the joint-
893 probability method, and distribution of hypocenters around the Yugama crater.
894 (a) Result of the joint-probability analysis. Black squares indicate seismic stations used
895 for the polarization analysis (KSE, KSHA, KSW, KSS).
896 (b) Distribution of hypocenters of high-frequency earthquakes during the same period as
897 the polarization analysis.
898 (c) Distribution of hypocenters of high-frequency earthquakes. Blue shows the 2014
899 unrest (January 2014 – December 2017), and red shows the 2018 unrest (January 2018 –
900 December 2023). The green rectangle shows the area of hypocenters used in panel (d).
901 (d) Spatiotemporal distribution of hypocenters projected onto the KSS–KSHA cross
902 section. Colors of the plots are the same as in panel (c).

Figure A1

Comparison between areal strain calculated from GEONET and that inferred from the volume change reported by Munekane (2021).

Gray circles show the raw areal strain calculated from GEONET.

The red line shows the areal strain after smoothing and removing the seasonal trend.

Orange circles show the areal strain calculated from the volume change reported by Munekane (2021).

Blue circles (right axis) show the volume change reported by Munekane (2021).

Figure B1

Schematic illustration of the calculation method for the polarization analysis and back-projection at each observation site.

Figure B2

Location of the SBL source estimated by polarization analysis and the joint-probability method.

(a) Joint probability of the SBL source location.

(b–e) Probability distributions estimated from the polarization analysis at KSHA, KSE, KSW, and KSS, respectively.

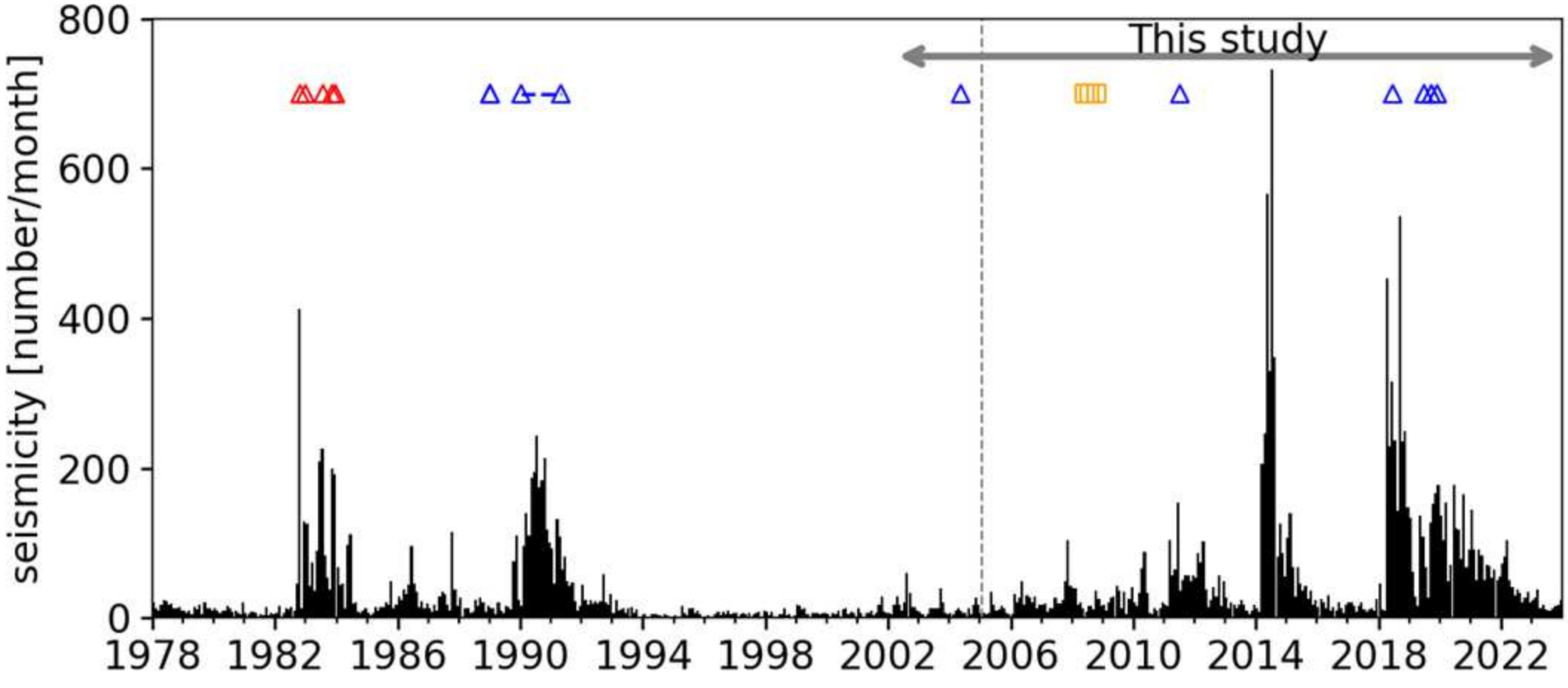
Black squares indicate seismic stations used for the polarization analysis (KSE, KSHA, KSW, KSS).

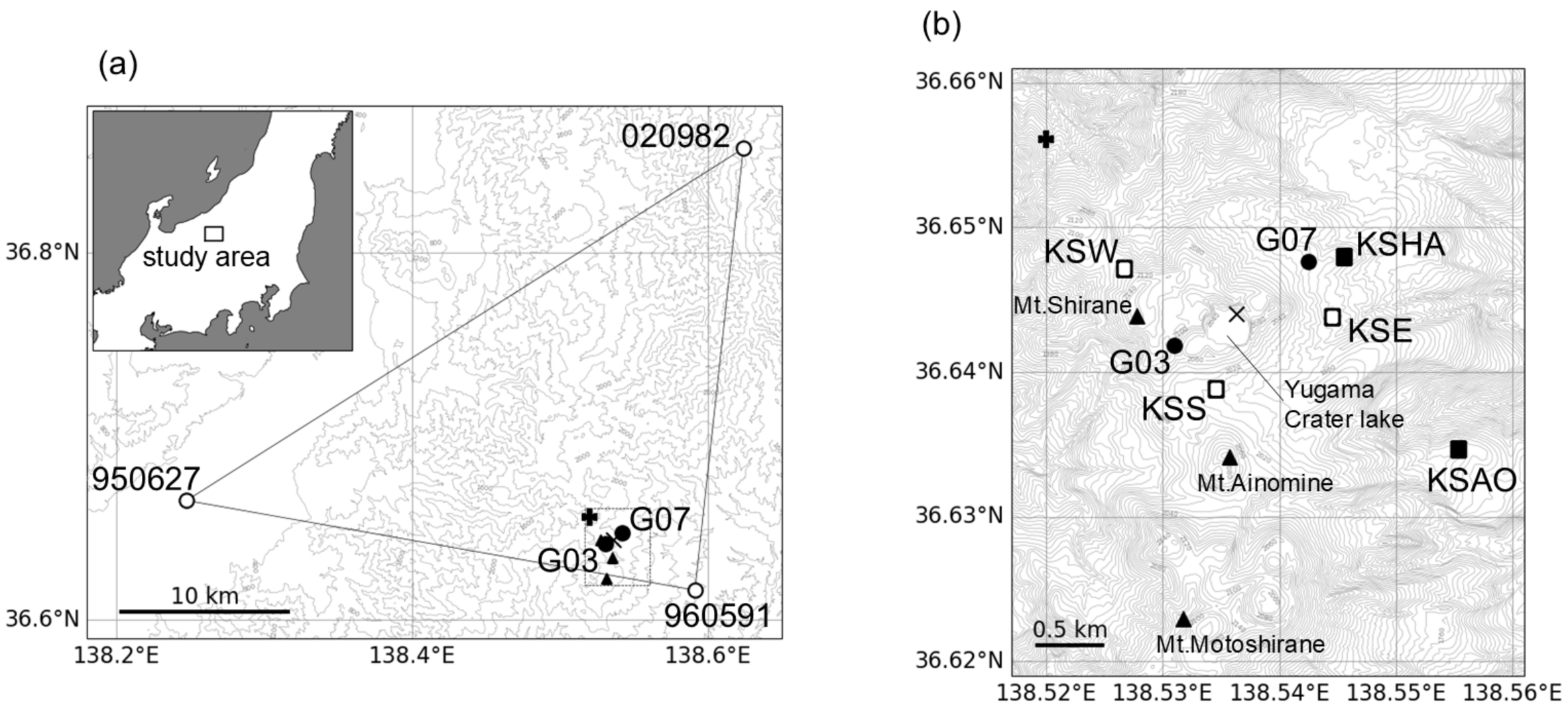
(a)


Kusatsu
400 km


Mt. Shirane
Yugama
Mt. Ainomine
Mt. Motoshirane
1 km
749 m
Image © 2025 Airbus
Google Earth

(b)

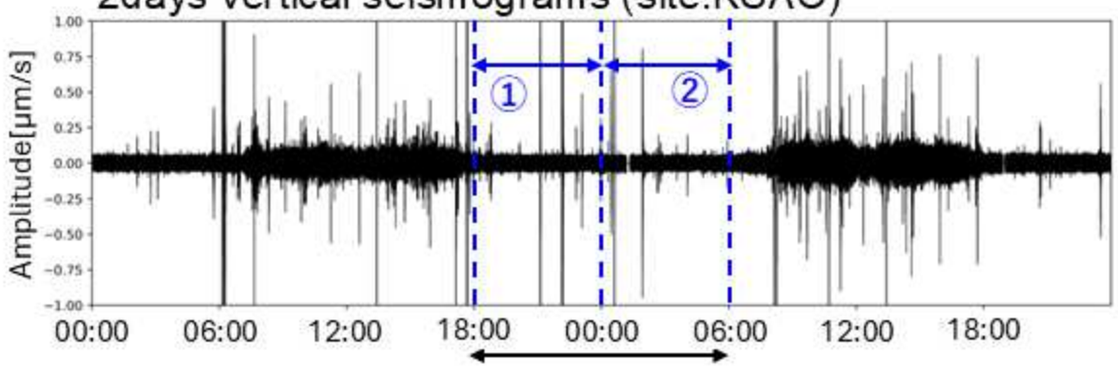

This study
seismicity [number/month]
800
600
400
200
0
1978
1982
1986
1990
1994
1998
2002
2006
2010
2014
2018
2022


(a)
study area
020982
950627
960591
G07
G03
10 km
36.8°N
36.6°N
138.2°E
138.4°E
138.6°E
(b)
36.66°N
36.65°N
36.64°N
36.63°N
36.62°N
KSW
G07
KSHA
Mt.Shirane
KSE
G03
KSS
Yugama
Crater lake
Mt.Ainomine
KSAO
0.5 km
Mt.Motoshirane
138.52°E
138.53°E
138.54°E
138.55°E
138.56°E

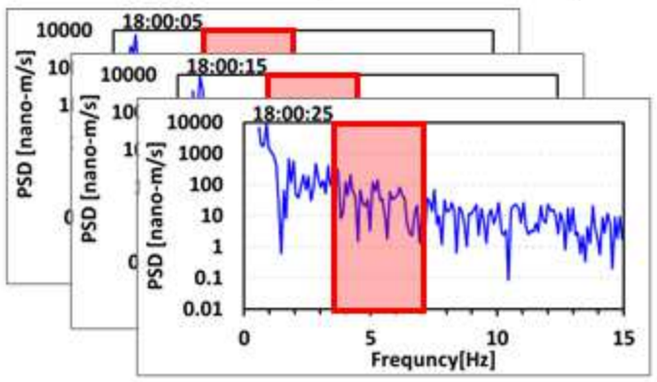
Flowchart of SBL calculation

(a) Step1: Daily calculation of raw SBL

2days vertical seismograms (site:KSAO)



Step1-1
Calculate power spectral density



power spectral density:

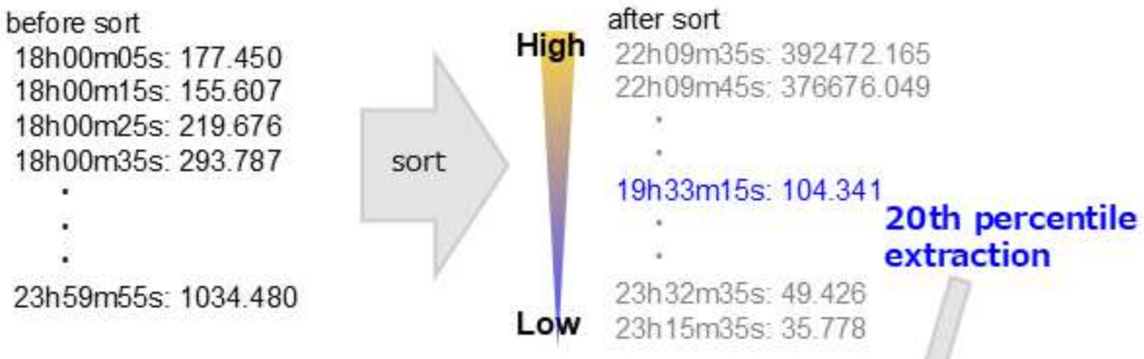
$$P_f(t,f)$$

time window: 10.24 s
shift: 10 s

Step1-2
calculate seismic power

$$Seismic\ Power\colon E(t) = \int_{3.5}^{7} P_f(t,f)\,df$$

Step1-3
Determine the value $E(t)$ that represents the day for each ①,②



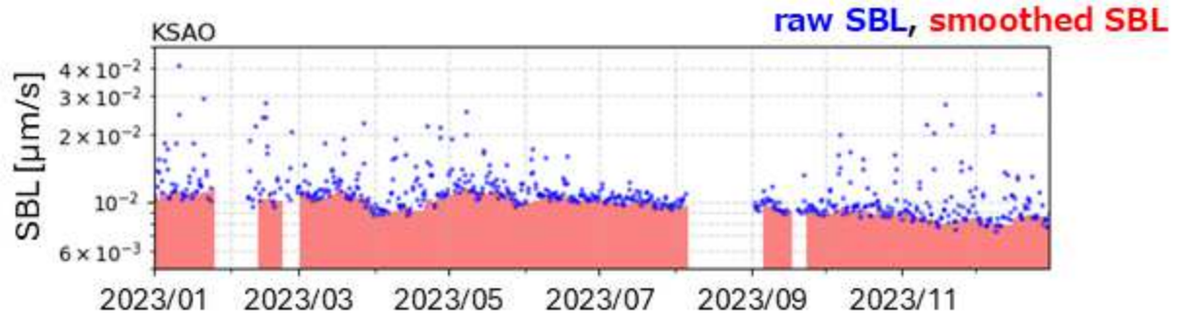
calculate raw SBL

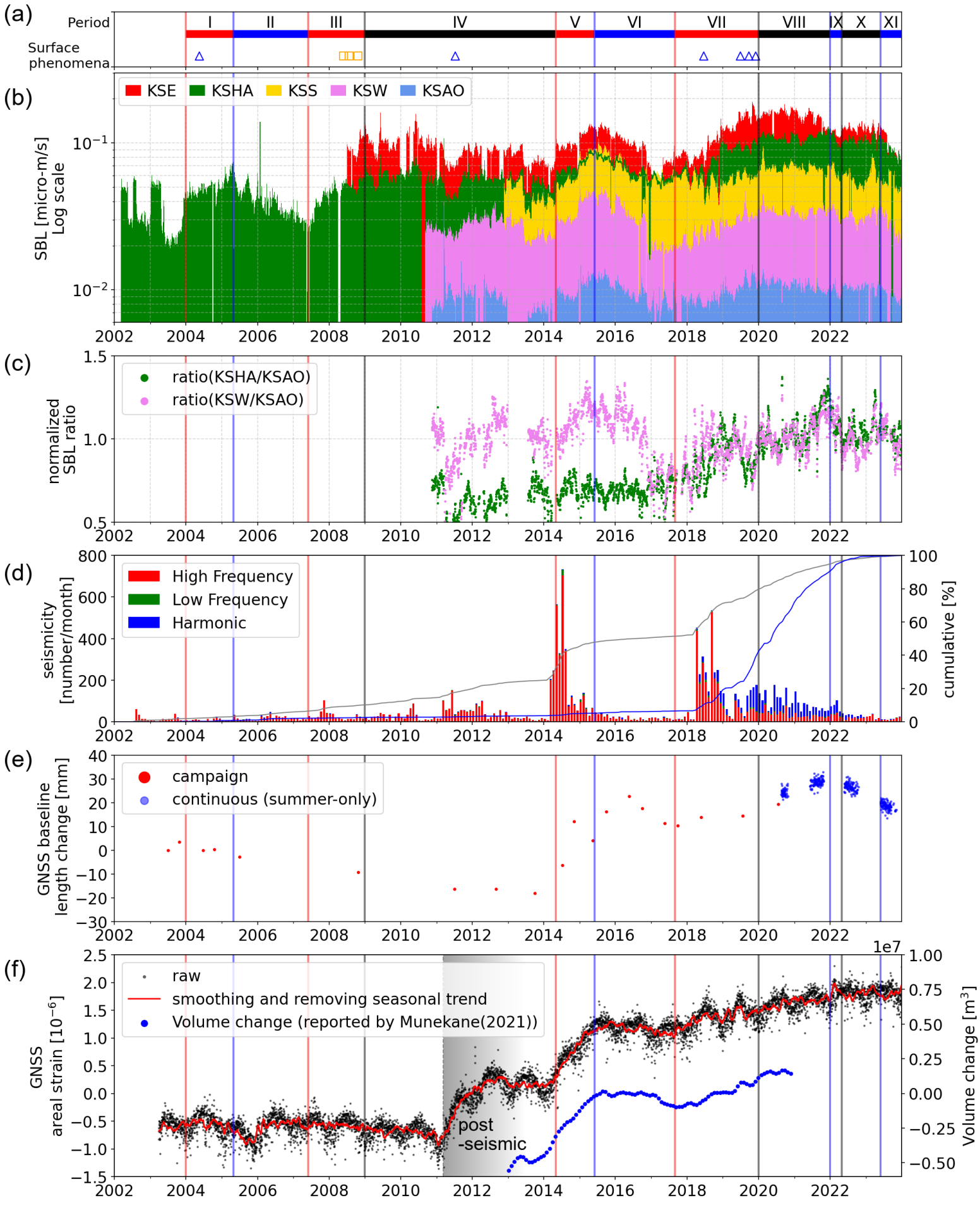
$$Seismic\ Background\ Level\colon SBL = \sqrt{E(t)}$$

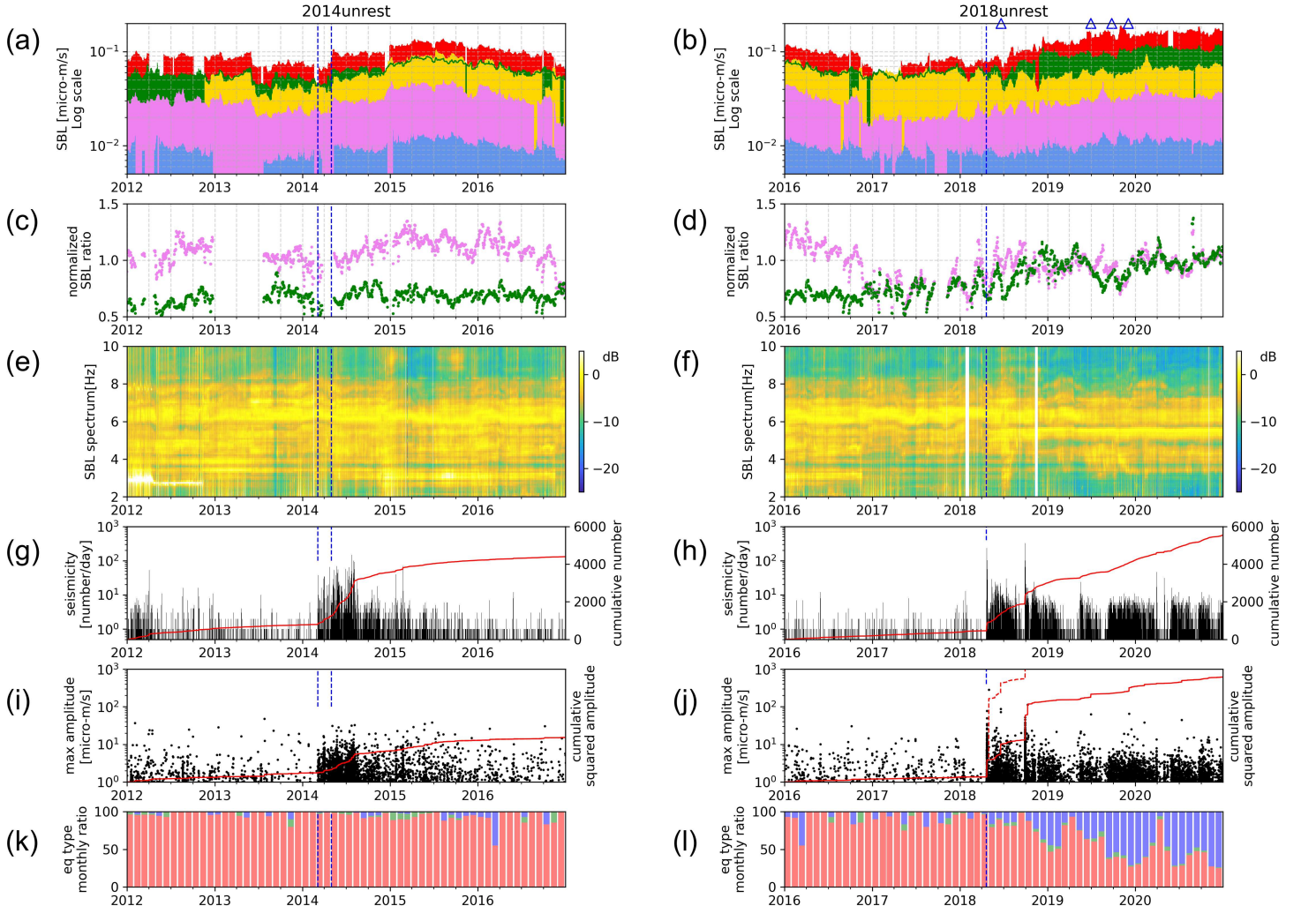
Time series

(b) Step2: calculate time series of smoothed SBL






(a)
Period
I
II
III
IV
V
VI
VII
VIII
IX
X
XI
Surface phenomena
(b)
KSE
KSHA
KSS
KSW
KSAO
SBL [micro-m/s]
Log scale
10^{-1}
10^{-2}
2002
2004
2006
2008
2010
2012
2014
2016
2018
2020
2022
(c)
ratio(KSHA/KSAO)
ratio(KSW/KSAO)
normalized SBL ratio
1.5
1.0
0.5
(d)
High Frequency
Low Frequency
Harmonic
seismicity [number/month]
800
600
400
200
0
cumulative [%]
100
80
60
40
20
0
(e)
campaign
continuous (summer-only)
GNSS baseline length change [mm]
40
30
20
10
0
−10
−20
−30
(f)
raw
smoothing and removing seasonal trend
Volume change (reported by Munekane(2021))
GNSS areal strain [10^{-6}]
2.5
2.0
1.5
1.0
0.5
0.0
−0.5
−1.0
−1.5
1e7
1.00
0.75
0.50
0.25
0.00
−0.25
−0.50
Volume change [m^3]
post
-seismic


2014unrest
2018unrest
(a)
(b)
(c)
(d)
(e)
(f)
(g)
(h)
(i)
(j)
(k)
(l)
SBL [micro-m/s]
Log scale
normalized
SBL ratio
SBL spectrum[Hz]
dB
seismicity
[number/day]
cumulative number
max amplitude
[micro-m/s]
cumulative
squared amplitude
eq type
monthly ratio

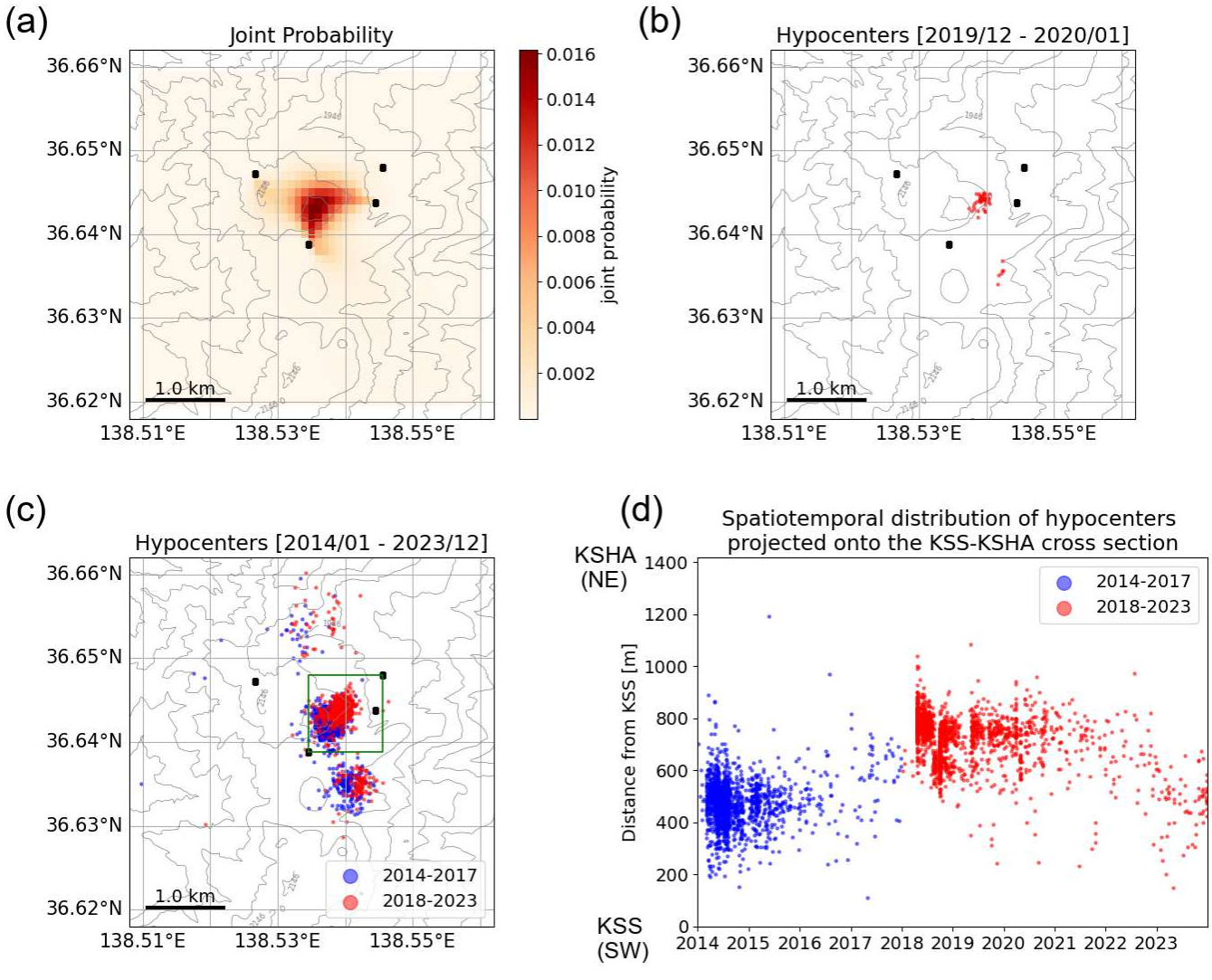

(a)
Joint Probability
36.66°N
36.65°N
36.64°N
36.63°N
36.62°N
138.51°E
138.53°E
138.55°E
1.0 km
0.016
0.014
0.012
0.010
0.008
0.006
0.004
0.002
joint probability
(b)
Hypocenters [2019/12 - 2020/01]
(c)
Hypocenters [2014/01 - 2023/12]
2014-2017
2018-2023
(d)
Spatiotemporal distribution of hypocenters
projected onto the KSS-KSHA cross section
KSHA
(NE)
KSS
(SW)
Distance from KSS [m]
1400
1200
1000
800
600
400
200
0
2014
2015
2016
2017
2018
2019
2020
2021
2022
2023

Table 1

Period	start	end	SBL
I	2004 (2004/1/1)	April 2005 (2005/4/30)	increase
II	around May 2005 (2005/5/1)	around May 2007 (2007/5/31)	decrease
III	around May 2007 (2007/6/1)	2008 (2008/12/31)	increase
IV	2009 (2009/1/1)	around May 2014 (2014/4/30)	no significant change
V	around May 2014 (2014/5/1)	around May 2015 (2015/5/31)	increase
VI	around May 2015 (2015/6/1)	mid-2017 (2017/8/31)	decrease
VII	late 2017 (2017/9/1)	around January 2020 (2019/12/31)	increase
VIII	January 2020 (2020/1/1)	around January 2022 (2021/12/31)	keeping high levels
IX	January 2022 (2022/1/1)	April 2022 (2022/4/30)	decrease *
X	May 2022 (2022/5/1)	May 2023 (2023/5/31)	no significant change
XI	around June 2023 (2023/6/1)		decrease

[footnote]

* The decrease in Period IX can be more clearly recognized when the results from KSE are also taken into account.

** Dates in parentheses correspond to the time intervals used for color coding in Fig. 4.

Table 2

	before 2014 unrest	2014 unrest	2018 unrest
SBL	2004 – around April 2005(Period-I): increase around May 2005 – around May 2007(Period-II): decrease around May 2007 – 2008 (Period-III): increase 2009 – around May 2014 (Period-IV): no significant change	2014/05 - 2015/05 (Period-V): increase 2015/05 - mid 2017 (Period-VI): decrease	late 2017 – 2020/01 (Period-VII): increase (In 2018, unstable) 2020/01 – 2022/01 (Period-VIII): keeping high levels 2022/01 – 2022/04 (Period-IX): decrease 2022/05 – 2023/05 (Period-X): no significant change
SBL spectrum	-	2014/03 - late2016: 3Hz 2014/05 - late2016: 4-5Hz	mid to late 2017-: 5-6Hz
Seismicity: (number, amplitude, type)	number: 2007/11 (Period-III) slight increase 2011 (Period-IV) slight increase type: High-frequency	number: 2014/03 increase 2014/05 further increase 2014/07 decrease type: High-frequency	number: 2018/04 rapidly increase amplitude: larger than 2014unrest type: High-frequency to harmonic
Ground deformation: Shallow source	not clearly identified	2014-2015: inflation	2018-2021: inflation
Ground deformation: Deep source	no volcanic signals	early 2014 - 2015: inflation	late 2017 - 2021: inflation

Supplementary Files

This is a list of supplementary files associated with this preprint. Click to download.

- Fig.A1ArealStrain20130101to20201231.png
- Fig.B1methodschematicillustrationbackazimuth.png
- Fig.B2jointprobabilityV.KSHAVI.KSEVI.KSWVI.KSS.png
- Fig.0graphicalabstractresized920300.png
- Supplementaryinformation.docx
- sblsmoothedV.KSAO2002010120231231.dat
- sblsmoothedV.KSHA2002010120231231.dat
- sblsmoothedVI.KSE2002010120231231.dat
- sblsmoothedVI.KSS2002010120231231.dat
- sblsmoothedVI.KSW2002010120231231.dat